Supporting Information

Guinn et al. 10.1073/pnas.1311948110

SI Materials

Determining ε- and α-Values. Values of ε_i (Eq. **2** and Table **1**) for hydrocarbon surface were determined from solubility data. Heat capacity data for the transfer of aliphatic hydrocarbons and benzene from the pure liquid to water and accessible surface area (ASA) values for these hydrocarbons (see, for example, refs. 1–4) were analyzed as in Eq. **1** to obtain ε_i values for aliphatic and aromatic surfaces. Using least-squares regression analysis (R, version 2.14.1), we obtain $\varepsilon_{aliphatic}$ = 0.35 ± 0.1 cal·mol⁻¹·K⁻¹·Å⁻² and $\varepsilon_{aromatic}$ = 0.25 ± 0.1 cal·mol⁻¹·K⁻¹·Å⁻². The value of ε_{amide} was previously determined by analysis of ΔC_p° for transfer of organic amides (2) using Eq. **1**. α_i-Values for interactions of urea and GuHCl with amide, aromatic C, and aliphatic C surface were determined from data for the interactions of these solutes with model compounds (5–7).

Because only two experimental quantities (one denaturant kinetic *m*-value and the corresponding activation ΔC_p°) are available for folding and for unfolding, only composite ΔASA

Predicting ΔASA$_{amide}$ and ΔASA$_{hydrocarbon}$ from ΔC_p° and an *m*-Value. To determine ΔASA$_{amide}$ and ΔASA$_{hydrocarbon}$ for proteins where ΔC_p° and either urea or GuHCl *m*-values were available, Eqs. **1** and **2** are rearranged to give the following:

$$\Delta\text{ASA}_x = \frac{\Delta Cp \times \alpha_y - m\text{-value} \times \varepsilon_y}{\varepsilon_x \times \alpha_y - \alpha_x \times \varepsilon_y}. \quad \textbf{[S1]}$$

In Eq. **S1**, the subscript *x* refers to the surface type for which the ASA is being determined (amide or hydrocarbon), and *y* refers to the remaining surface type. The coefficients α_x and α_y are the α-values for the solute for which the *m*-value used in Eq. **S1** was determined. ΔCp and *m*-values from folding kinetic data give ΔASA for the U → transition state (TS) transition, whereas values from unfolding data give ΔASA for the TS → F transition.

From Eq. **S1**, we obtain the following expressions for θ_{ASA}^{TS}, the degree of advancement of the TS, and Ω^{TS}, the preferential burial of hydrocarbon surface:

$$\theta_{\text{ASA}}^{U \to TS} = \frac{\Delta\text{ASA}_{U \to TS}}{\Delta\text{ASA}_{U \to F}} = \frac{\Delta Cp_{U \to TS}(\alpha_y - \alpha_x) - m\text{-value}_{U \to TS}(\varepsilon_y + \varepsilon_x)}{\Delta Cp_{U \to TS}(\alpha_y - \alpha_x) - m\text{-value}_{U \to TS}(\varepsilon_y + \varepsilon_x) + \Delta Cp_{TS \to F}(\alpha_y - \alpha_x) - m\text{-value}_{TS \to F}(\varepsilon_y + \varepsilon_x)} \quad \textbf{[S2]}$$

$$\Omega_z = \frac{r_z}{r_{U \to F}} = \frac{(\Delta Cp_z \times \alpha_y - m\text{-value}_z \times \varepsilon_y)/(\Delta Cp_z \times \alpha_x - m\text{-value}_z \times \varepsilon_x)}{(\Delta Cp_z \times \alpha_y - m\text{-value}_z \times \varepsilon_y + \Delta Cp_b \times \alpha_y - m\text{-value}_b \times \varepsilon_y)/(\Delta Cp_z \times \alpha_x - m\text{-value}_z \times \varepsilon_x + \Delta Cp_b \times \alpha_x - m\text{-value}_b \times \varepsilon_x)}. \quad \textbf{[S3]}$$

values for hydrocarbon and amide surfaces are obtainable from these data. To determine composite ε- and α-values for the hydrocarbon surface buried in protein folding, we used the average ratio of aliphatic:aromatic ΔASA values (9.3:1) obtained for unfolding of a large set of globular proteins (7). [For the 13 proteins analyzed here, the average ratio is 9.6. Although the range is large (4–27), this has little consequence for the composite ε- and α-values because the aliphatic contribution is always dominant.] To determine composite α-values for urea for the amide O and N surface buried in protein folding, we used the average ratio of amide O:amide N ΔASA values (2.4:1) obtained for unfolding of the same large set of globular proteins (7). [For the 13 proteins analyzed here, the average ratio is 2.7. Although the range is moderately large (2–5), its effect on the composite α-value for urea is not outside of the propagated uncertainty.] Only composite values are available for the α-coefficient for interaction of GuHCl with amide (O,N) ASA, and for the ε-coefficient for the contribution of amide (O,N) ASA to ΔC_p°. The GuHCl-amide (O,N) α-value was obtained from studies with secondary amides, whereas the ΔC_p°-amide ε-value was obtained from studies with primary amides. Data are not currently available to refine these coefficients, and the agreement between predicted and structural values for the amide ΔASA of folding from U to F (Table 2 and Fig. 3) indicates the coefficients used are sufficiently accurate for this analysis.

In Eq. **S3**, the subscript *x* refers to hydrocarbon surface and *y* refers to amide surface. The subscript *z* refers to the transition for which Ω is being determined (U → TS or TS → F) and *b* refers to the remaining transition.

For Eqs. **S1–S3**, uncertainty was determined using standard propagation methods for independent variables:

$$\begin{aligned}
s_f^2 = {} & \left(\frac{\partial F}{\partial \Delta Cp_{U \to TS}}\right)^2 s_{\Delta Cp_{U \to TS}}^2 + \left(\frac{\partial F}{\partial \Delta Cp_{TS \to F}}\right)^2 s_{\Delta Cp_{TS \to F}}^2 \\
& + \left(\frac{\partial F}{\partial \Delta m\text{-value}_{U \to TS}}\right)^2 s_{m\text{-value}_{U \to TS}}^2 \\
& + \left(\frac{\partial F}{\partial m\text{-value}_{TS \to F}}\right)^2 s_{\Delta m\text{-value}_{TS \to F}}^2 + \left(\frac{\partial F}{\partial \alpha_x}\right)^2 s_{\alpha_x}^2 \\
& + \left(\frac{\partial F}{\partial \alpha_y}\right)^2 s_{\alpha_y}^2 + \left(\frac{\partial F}{\partial \varepsilon_x}\right)^2 s_{\varepsilon_x}^2 + \left(\frac{\partial F}{\partial \varepsilon_y}\right)^2 s_{\varepsilon_y}^2, \quad \textbf{[S4]}
\end{aligned}$$

where *F* is the variable for which uncertainty is being determined. For each protein, Eq. **S4** was solved using MATLAB to determine uncertainties in ΔASA, θ and Ω values.

Uncertainties (Table 2) are typically larger for amide ΔASA (12–30%) than for hydrocarbon ΔASA (5–20%), and amide uncertainties are typically larger when determined from urea *m*-values than from GuHCl *m*-values (30% vs. 14%).

Surface Area Calculations. Values of ΔASA for unfolding, 1FKD, 1CQU, and 2CRO assuming an extended denatured state were obtained from Guinn et al. (7). Values of ΔASA for unfolding all other globular proteins and the model β-hairpin were calculated by building extended polypeptides and analyzing amount and composition of the ASA of this extended structure and the native structure by Surface Racer (9) using Richards van der Waals radii. Folded-state ASAs were calculated from structures in the Protein Data Bank (PDB) (10). Unfolded proteins and unfolded regions in folding intermediates and in TS were modeled by using the extended conformation of the backbone generated using Pymol ($\varphi = 180$, $\psi = 180$) and with statistically preferred side-chain rotamers chosen among common rotamers [with Coot (11)] to avoid steric clashes. To build models of possible intermediates with all of the native secondary structure (I_{ss}) and more advanced models (I_{pre}, TS) we started with F and changed the disposition of secondary structural elements to minimize their interactions with each other by changing the backbone conformations of intervening regions. Two or more α-helices or β-sheets that were connected by short hairpins were considered to be one secondary structural element and moved as a rigid body.

Possible Sources of Systematic or Random Error in Predicted and Structural ΔASA Values in Fig. 1 and Fig. S1. In Fig. 1*A*, the three proteins with the largest discrepancies between experimentally predicted and structural values of amide ΔASA_A are FKBP (1FKD), ACP-1 (2VH7), and 434 Cro (2CRO). In all three cases, the experimentally predicted value is larger in magnitude than the structural value. Because the structural value is calculated for an extended model of the unfolded polypeptide and therefore is the maximum magnitude of amide ΔASA_A, the model of the unfolded form is not the origin of these systematic discrepancies. In Fig. 1*B*, the four proteins with the largest deviation between structural and predicted values of ΔASA_H are T4L (1B61), PLB1 (1HZ6), Bs-Csp (1NMG), and Bc-Csp (1CO9). In all four cases, the experimentally predicted value is smaller in magnitude than the structural value. Although the existence of residual structure in the unfolded peptide could explain these discrepancies, such structure should also bury amide ASA, but experimentally determined ΔASA_A values for these proteins do not deviate significantly from the line in Fig. 1*A*. Fig. S1 shows a similar level of agreement between the experimentally determined and structural values for the sum of ΔASA_A and ΔASA_H to that in Fig. 1*B* for ΔASA_H, as expected because ΔASA_H is the dominant term in the sum.

Another possible source of systematic uncertainty is from the analysis of heat capacity changes and denaturant *m*-values entirely in terms of hydrocarbon (aliphatic plus aromatic) and amide (N plus O) surface. This not only ignores potential contributions from other surface types (which account for ∼10% of the ΔASA in protein folding from an extended polypeptide) but also ignores any effect of systematic differences between proteins in the ratio of aliphatic to aromatic hydrocarbon and/or of amide N to amide O buried in folding to and from TS. This effect by itself does not appear capable of explaining the differences discussed above. To test the reproducibility of the extended-chain models of the unfolded state, in which the choice of side-chain rotamers is based on avoiding clash as described above, two such models for 2CRO and 1NMG were independently built and analyzed by Surface Racer. Values of hydrocarbon and amide ASA for the two models of each protein agree within 5%, indicating that ambiguity in the extended-chain model is also not a factor in these analyses.

Amide Surface Buried in Forming Secondary Structure of Representative Proteins. For 434 Cro (all α-helix), the amide ΔASA per residue buried in α-helix formation (20 $A^2 \cdot res^{-1}$) is almost the same as that calculated for the $(AEAAKA)_n$ α-helical peptide (22 $A^2 \cdot res^{-1}$). For 1POH, which contains nearly equal amounts of α-helix and β-sheet, the amide ΔASA per residue buried in secondary structure formation (17 res^{-1}) is halfway between the values calculated for $(AEAAKA)_n$ α-helical peptide and PDB ID code 2EVQ β-hairpin. For Bs-Csp (all β-structure), the amide ΔASA per residue (17 $A^2 \cdot res^{-1}$) is somewhat larger than that of the PDB ID code 2EVQ β-hairpin (12 $A^2 \cdot res^{-1}$) because the Bs-Csp sheets involve both local and distant interactions.

1. Spolar RS, Record MT, Jr. (1994) Coupling of local folding to site-specific binding of proteins to DNA. *Science* 263(5148):777–784.
2. Spolar RS, Livingstone JR, Record MT, Jr. (1992) Use of liquid hydrocarbon and amide transfer data to estimate contributions to thermodynamic functions of protein folding from the removal of nonpolar and polar surface from water. *Biochemistry* 31(16):3947–3955.
3. Livingstone JR, Spolar RS, Record MT, Jr. (1991) Contribution to the thermodynamics of protein folding from the reduction in water-accessible nonpolar surface area. *Biochemistry* 30(17):4237–4244.
4. Privalov PL, Gill SJ (1988) Stability of protein structure and hydrophobic interaction. *Adv Protein Chem* 39:191–234.
5. Pegram LM, Record MT, Jr. (2008) Thermodynamic origin of hofmeister ion effects. *J Phys Chem B* 112(31):9428–9436.
6. Pegram LM, et al. (2010) Why Hofmeister effects of many salts favor protein folding but not DNA helix formation. *Proc Natl Acad Sci USA* 107(17):7716–7721.
7. Guinn EJ, Pegram LM, Capp MW, Pollock MN, Record MT, Jr. (2011) Quantifying why urea is a protein denaturant, whereas glycine betaine is a protein stabilizer. *Proc Natl Acad Sci USA* 108(41):16932–16937.
8. Hong J, Capp MW, Saecker RM, Record MT, Jr. (2005) Use of urea and glycine betaine to quantify coupled folding and probe the burial of DNA phosphates in lac repressor-lac operator binding. *Biochemistry* 44(51):16896–16911.
9. Tsodikov OV, Record MT, Jr., Sergeev YV (2002) Novel computer program for fast exact calculation of accessible and molecular surface areas and average surface curvature. *J Comput Chem* 23(6):600–609.
10. Berman HM, et al. (2000) The Protein Data Bank. *Nucleic Acids Res* 28(1):235–242.
11. Emsley P, Lohkamp B, Scott WG, Cowtan K (2010) Features and development of Coot. *Acta Crystallogr D Biol Crystallogr* 66(Pt 4):486–501.
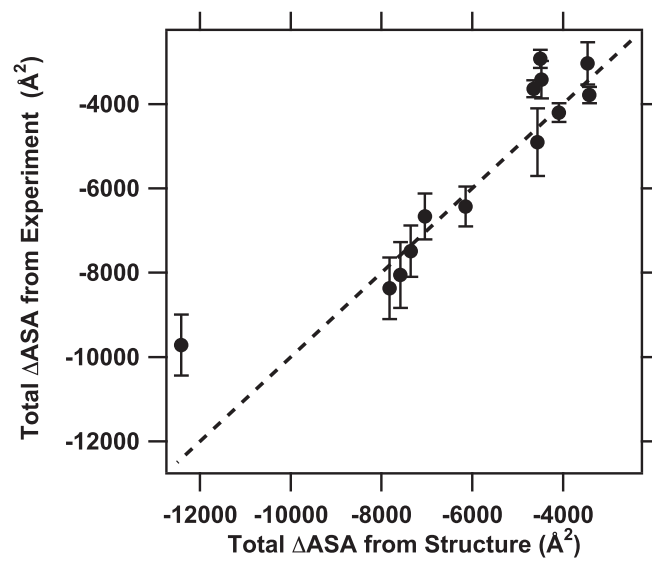
Fig. S1. Total (amide plus hydrocarbon) ΔASA values for the U → F transition for 13 proteins from thermodynamic data (Eqs. **1** and **2**) compared with values calculated from structural data (Table 2). The line represents equality of predicted and structural values.

Table S1. Literature values for activation ΔC_p°, urea and GuHCl folding m-values, and folding and unfolding rate constants

Protein*	Size[†]	Activation ΔC_p°, cal·K⁻¹·mol⁻¹ U → TS	TS → F	Urea m-value, cal·mol⁻¹·M⁻¹ U → TS	TS → F	GuHCl m-value, cal·mol⁻¹·M⁻¹ U → TS	TS → F	Rate constant, s⁻¹ Fold, k_f	Unfold
NTL9 (1)	56	−370 ± 110	−280 ± 110			888 ± 124	610 ± 83	1.1×10^3	0.53
Bc-Csp (2)	66	−500 ± 10	−290 ± 10			1,551 ± 78[‡]	189 ± 9[‡]	1.1×10^3	29
Bs-Csp (3)	67	−650 ± 70	−70 ± 100	640 ± 32[§]	24 ± 1[§]			1.1×10^3	29
Fyn SH3 (4)	58 (67)	−444 ± 10	−420 ± 5			1,090 ± 12	518 ± 12	94	9.9×10^{-4}
434 Cro (5)	65 (71)	−730 ± 160	−270 ± 190	830 ± 58	140 ± 12			2.0×10^2	0.59
PLB1 (6, 7)	67 (72)	−320 ± 20	−190 ± 30			1,400 ± 18	598 ± 12	61	0.30
CI2 (8, 9)	65 (83)	−490 ± 10	−480 ± 20			1,042 ± 12	692 ± 12	72	1.4×10^{-4}
HPr (10)	85	−770 ± 40	−730 ± 110			1,653 ± 83[‡]	919 ± 46[‡]	15	2.1×10^{-3}
ACP (11)	98	−610 ± 40	−910 ± 50	962 ± 30	251 ± 6			0.23	1.1×10^{-4}
ACP-1 (12)	99	−590 ± 60	−890 ± 90	1,219 ± 60	478 ± 18			2.3	1.5×10^{-3}
RPS6 (13, 14)	101	−902 ± 92	−973 ± 138			1,650 ± 14	736 ± 14	3.3×10^2	3.1×10^{-6}
FKBP (15)	107	−670 ± 10	−1,040 ± 80	1,107 ± 36	544 ± 36	(6,569 ± 178)[§]	(3,196 ± 118)[§]	4.3	1.7×10^{-4}
T4L (16)	164	−1,630 ± 163[¶]	−550 ± 55[¶]			3,311 ± 166[‡]	−979 ± 49[‡]	4.5×10^{-3}	6.5×10^{-4}

*Reference given is source for kinetic data (ΔC_p°, m-values, rate constants). Proteins are ordered by total number of residues.

[†]Size is given as number of residues. For proteins with an unstructured region, number of structured residues is given first and total number of residues is given in parentheses.

[‡]SE not reported; assigned as 5% based on average of errors reported for other m-values.

[§]GuHCl thermodynamic m-value for 1FKD (9765 cal·mol⁻¹·M⁻¹) appears unusually large by comparison with the value predicted from the structure (2,131 cal·mol⁻¹·M⁻¹; Table S3), so GuHCl kinetic m-values are not analyzed.

[¶]SE not reported; assigned as 10% based on average of errors reported for other ΔC_p° values.

1. Kuhlman B, Luisi DL, Evans PA, Raleigh DP (1998) Global analysis of the effects of temperature and denaturant on the folding and unfolding kinetics of the N-terminal domain of the protein L9. *J Mol Biol* 284(5):1661–1670.
2. Perl D, et al. (2002) Thermodynamics of a diffusional protein folding reaction. *Biophys Chem* 96(2–3):173–190.
3. Schindler T, Schmid FX (1996) Thermodynamic properties of an extremely rapid protein folding reaction. *Biochemistry* 35(51):16833–16842.
4. Plaxco KW, et al. (1998) The folding kinetics and thermodynamics of the Fyn-SH3 domain. *Biochemistry* 37(8):2529–2537.
5. Laurents DV, et al. (2000) Folding kinetics of phage 434 Cro protein. *Biochemistry* 39(45):13963–13973.
6. Scalley ML, Baker D (1997) Protein folding kinetics exhibit an Arrhenius temperature dependence when corrected for the temperature dependence of protein stability. *Proc Natl Acad Sci USA* 94(20):10636–10640.
7. Kim DE, Fisher C, Baker D (2000) A breakdown of symmetry in the folding transition state of protein L. *J Mol Biol* 298(5):971–984.
8. Jackson SE, Fersht AR (1991) Folding of chymotrypsin inhibitor 2. 2. Influence of proline isomerization on the folding kinetics and thermodynamic characterization of the transition state of folding. *Biochemistry* 30(43):10436–10443.
9. Tan YJ, Oliveberg M, Fersht AR (1996) Titration properties and thermodynamics of the transition state for folding: Comparison of two-state and multi-state folding pathways. *J Mol Biol* 264(2):377–389.
10. Van Nuland NAJ, et al. (1998) Slow cooperative folding of a small globular protein HPr. *Biochemistry* 37(2):622–637.
11. Chiti F, et al. (1998) Structural characterization of the transition state for folding of muscle acylphosphatase. *J Mol Biol* 283(4):893–903.
12. Taddei N, et al. (1999) Thermodynamics and kinetics of folding of common-type acylphosphatase: Comparison to the highly homologous muscle isoenzyme. *Biochemistry* 38(7):2135–2142.
13. Otzen DE, Kristensen O, Proctor M, Oliveberg M (1999) Structural changes in the transition state of protein folding: Alternative interpretations of curved chevron plots. *Biochemistry* 38(20):6499–6511.
14. Otzen DE, Oliveberg M (2004) Correspondence between anomalous m- and DeltaCp-values in protein folding. *Protein Sci* 13(12):3253–3263.
15. Main ERG, Fulton KF, Jackson SE (1999) Folding pathway of FKBP12 and characterisation of the transition state. *J Mol Biol* 291(2):429–444.
16. Chen BL, Baase WA, Schellman JA (1989) Low-temperature unfolding of a mutant of phage T4 lysozyme. 2. Kinetic investigations. *Biochemistry* 28(2):691–699.

Table S2. Values of $\theta_C^{U \to TS}$, $\theta_{ASA}^{U \to TS}$, and $\theta_m^{U \to TS}$ quantifying fraction of overall ΔC_p°, ΔASA, or m-value observed for U → TS

Protein	$\theta_C^{U \to TS} = \Delta C p_{U \to TS} / \Delta C p_{U \to F}$	$\theta_{ASA}^{U \to TS}$ (Eq. 4)	$\theta_m^{U \to TS} = m\text{-value}_{U \to TS} / m\text{-value}_{U \to F}$
NTL9	0.57 ± 0.07	0.58 ± 0.08	0.59 ± 0.03
Bc-Csp	0.63 ± 0.00	0.71 ± 0.01	0.89 ± 0.00
Bs-Csp	0.90 ± 0.01	0.94 ± 0.05	0.96 ± 0.00*
FynSH3	0.51 ± 0.01	0.56 ± 0.01	0.68 ± 0.00
434 Cro	0.73 ± 0.04	0.81 ± 0.06	0.86 ± 0.01*
PLB1	0.63 ± 0.01	0.66 ± 0.02	0.70 ± 0.00
CI2	0.51 ± 0.01	0.53 ± 0.01	0.60 ± 0.00
HPr	0.51 ± 0.01	0.55 ± 0.04	0.64 ± 0.01
ACP	0.40 ± 0.02	0.62 ± 0.03	0.79 ± 0.01*
ACP-1	0.40 ± 0.02	0.60 ± 0.03	0.72 ± 0.01*
RPS6	0.48 ± 0.03	0.53 ± 0.04	0.69 ± 0.00
FKBP	0.42 ± 0.01	0.56 ± 0.02	0.67 ± 0.01*
T4L	0.75 ± 0.02	0.75 ± 0.02	0.77 ± 0.01

*Determined from urea m-values; $\theta_m^{U \to TS}$ for GuHCl m-value is even larger; therefore, the inequality $\theta_m^{U \to TS} > \theta_C^{U \to TS}$ is valid independently of which m-value (GuHCl or urea) is used.

Table S3. Values of the hydrocarbon/amide ΔASA ratio r and corresponding Ω values

Protein PDB ID code	$r = \Delta ASA_H/\Delta ASA_A$		Ω (Fig. 3; Eq. 5)	
	U → TS	TS → F	U → TS	TS → F
NTL9	2.72	2.92	0.97 ± 0.16	1.04 ± 0.24
Bc-Csp	2.25	6.83	0.78 ± 0.02	2.35 ± 0.26
Bs-Csp	2.48	*	0.92 ± 0.17	*
FynSH3	2.66	4.45	0.81 ± 0.02	1.36 ± 0.05
434 Cro	2.09	*	0.83 ± 0.20	*
PBL1	1.75	2.23	0.92 ± 0.04	1.17 ± 0.10
CI2	2.98	3.97	0.88 ± 0.02	1.17 ± 0.03
HPr	2.95	4.37	0.85 ± 0.05	1.25 ± 0.09
ACP	1.50	*	0.46 ± 0.06	*
ACP-1	1.20	6.81	0.58 ± 0.06	3.29 ± 1.20
RPS6	3.33	6.20	0.77 ± 0.06	1.43 ± 0.10
FKBP	1.44	7.26	0.57 ± 0.06	2.85 ± 1.03
T4L	3.08	3.40	0.98 ± 0.03	1.07 ± 0.10

*Omitted due to small magnitude of ΔASA and >100% uncertainty in ΔASA_A for TS → F transition.

Table S4. Comparisons of values of ΔASA, $\theta_{ASA}^{U \to X}$, $r_{U \to X}$, and $r_{X \to F}$ determined from structural models of intermediates I_{ss}, I_{pre}, and TS (symbolized by X) with values determined from m-value, ΔC_p° analysis (Table 2 and Tables S1 and S2) for 434 Cro, HPr, and Bs-Csp

Protein	ASA source*	$\Delta ASA_H^{U \to X}$	$\Delta ASA_A^{U \to X}$	$\theta_{ASA}^{U \to X}$ (Eq. 4)	$r_{U \to X}$	$r_{X \to F}$
434 Cro	m-value, ΔC_p°	−2,673	−1,278	0.81	2.09	ND
(2CRO)	Model I_{ss}	−1,627	−796	0.50	2.04	6.70
	Model I_{pre}	−2,054	−802	0.59	2.56	5.42
	TS model	−2,578	−972	0.74	2.65	8.39
HPr	m-value, ΔC_p°	−2,629	−890	0.55	2.95	4.37
(1POH)	Model I_{ss}	−1,649	−876	0.40	1.88	4.63
	TS model	−1,817	−818	0.43	2.22	4.01
Bs-Csp	m-value, ΔC_p°	−2,292	−923	0.94	2.48	ND
(1NMG)	Model $I_{ss}^{\dagger}$	−1,535	−503	0.46	3.05	3.43
	Model I_{pre}	−2,112	−606	0.61	3.49	2.93
	TS model	−3,121	−937	0.91	3.33	2.61

*Models for 434 Cro and Bs-Csp intermediates (I_{ss} and I_{pre}) and TS shown in Fig. 4. See Fig. 4 legend and accompanying text for characteristics used to model these species.
†For Bs-Csp, the strands of one β-sheet are not contiguous and the intervening regions cannot be modeled as extended in I_{ss}.

Table S5. Number of residues in α-helices and β-sheets, predicted backbone amide ΔASA for formation of all native 2° structure (ss), and ratio of the total amide ΔASA for U → TS obtained from analysis of folding kinetics (Table 2) to the backbone amide ΔASA from 2° structure formation

Protein PDB ID code	No. α-helical residues	No. β-sheet residues	Predicted backbone amide ΔASA from 2° structure formation*	$\Delta ASA_{A,U \to TS}$/backbone amide ΔASA_{ss}
1CQU	18	11	−528	0.9
1C9O	3	41	−558	1.4
1NMG	0	30	−360	2.6
1NYF	3	27	−390	1.5
2CRO	40	0	−880	1.5
1HZ6	21	28	−798	0.9
2CI2	14	18	−524	1.1
1POH	29	23	−914	1.0
1APS	18	36	−828	2.0
2VH7	24	41	−1,020	2.1
1RIS	28	47	−1,180	0.8
1FKD	14	43	−824	2.3
1B6I	106	15	−2,512	0.7

*Calculated using per-residue backbone amide ΔASA of −22 Å² for α-helix and −12 Å² β-hairpin (see text).